Quantitative visualization of colloidal and intracellular gold nanoparticles by confocal microscopy

Sabine Klein
Friedrich-Loeffler-Institut Mariensee
Institute of Farm Animal Genetics
Federal Research Institute of Animal Health
Höltystr. 10
D-31535 Neustadt, Germany

Svea Petersen
LaserZentrum Hannover e.V.
Hollerithallee 8
D-30149 Hannover, Germany

Ulrike Taylor
Detlef Rath
Friedrich-Loeffler-Institut Mariensee
Institute of Farm Animal Genetics
Federal Research Institute of Animal Health
Höltystr. 10
D-31535 Neustadt, Germany

Stephan Barcikowski
LaserZentrum Hannover e.V.
Hollerithallee 8
D-30149 Hannover, Germany

Abstract. Gold nanoparticles (AuNPs) have the potential to become a versatile biomarker. For further use of AuNPs labeled with functionalized molecules, their visualization in biological systems by routine laboratory tools such as light microscopy is crucial. However, the size far below the diffraction limit affords specialized parameters for microscopical detection, which stimulated the current study, aimed to determine from which size onward AuNPs, either in dispersion or cell-associated, can be reliably detected by standard confocal microscopy. First, gold colloids of size-restricted fractions are examined in dispersion. At a minimum particle size of 60 nm, detection appears to be reliable. Particle counts in dilution series confirm these results by revealing single particle detection of 60-nm colloids. Second, AuNPs are visualized and quantified in cells, which interestingly cause a phase shift in the reflection of AuNPs. Gold mass spectroscopy confirms the number of AuNPs counted microscopically inside cells. Furthermore, it demonstrates for the first time a very high diffusion rate of 15-nm particles into the cells. In conclusion, the results back the suitability of confocal microscopy for the quantitative tracking of colloidal and intracellular gold nanoparticles sized 60 nm. *© 2010 Society of Photo-Optical Instrumentation Engineers.* [DOI: 10.1117/1.3461170]

Keywords: microscopy; confocal optics; scattering; mass spectroscopy; dispersion; gold nanoparticles.

Paper 09563PR received Dec. 18, 2009; revised manuscript received Mar. 28, 2010; accepted for publication Apr. 12, 2010; published online Jul. 2, 2010.

1 Introduction

The visualization of nanomarkers has gained increasing importance in the fast developing area of biomedical imaging. As the absorption and scattering cross sections of metal nanoparticles are several orders of magnitude higher compared to fluorescing organic dyes,[1–3] metal nanoparticles have the potential to become very efficient biomarkers. Among these, laser-generated colloidal gold nanoparticles appear to be biocompatible[4] and are fairly easily bioconjugated for further functionalization.[5] Additionally, metal nanoparticles do not suffer from photobleaching, and their extinction spectrum can be tuned by changing their size and shape.[2] However, their size far below the diffraction limit affords special conditions for optical detection. Furthermore, *in vivo* applications in cellular systems afford detection systems not compromising the viability of the cells. Various approaches for the visualization of AuNPs have been described recently.[6–8] Many of these, such as dark and near-field light microscopy and confocal microscopy (LSCM), are based on the surface plasmon resonance (SPR)-enhanced scattering of AuNPs.[7–9] However, so far all reported approaches of single particle detection were performed with fixed nanoparticles. Thus, single 40-nm-sized particles[8,10,11] were successfully visualized fixed on a glass surface, but not in a colloid. Besides SPR-enhanced scattering, SPR-enhanced absorption can be used for the visualization of AuNPs. While the scattering cross section is high for particles larger than 50 nm, for particles smaller than 30 nm the absorption prevails, and scattering is practically not apparent for visualization of particles with diameters of less than 20 nm according to the Mie theory.[3,6] Lindfors et al. demonstrated both detection methods again for fixed AuNPs between 5 and 100 nm by applying a supercontiuum white light confocal microscopy.[12] They recorded size-dependent scattering and absorption spectra using either a piezoelectric element and a charge-coupled device (CCD) camera or an imaging spectrometer. This study demonstrated surface-fixed particles larger than 50 nm as suitable for detection by their scattering cross sections and confirmed previous data.[1,2]

However, the visualization and quantification of AuNPs as nanomarkers in biological systems does not allow for AuNP fixation on a surface. Consequently, the visualization of nanoparticles in dispersion is required, which might have a variety of implications on imaging parameters. Additionally important for visualization in biological systems is the suspected red shift of AuNP SPR that generally occurs with increasing refractive index of the surrounding medium.[13] Thus, the aim of the current study was to define parameters allowing the visualization and quantification of colloidal and intracellular laser-generated AuNPs by conventional confocal microscopy, which represents a standard laboratory tool.

Address all correspondence to: Sabine Klein, Tel: +495034 871186; Fax: +495034 87143; E-mail: sabine.klein@fli.bund.de; and Stephan Barcikowski, Tel: +49511 2788377; Fax: +49511 2788100; E-mail: s.barcikowski@lzh.de.

1083-3668/2010/15(3)/036015/11/$25.00 © 2010 SPIE

AuNP colloids were excited with continuous single wavelength laser excitation, and the light microscopic limits of AuNP visualization by SPR-enhanced light scattering and photoluminescence were investigated. The size-dependent visibility of the AuNPs was studied in two different series: while the first series was adjusted to a constant mass (CM), the second series was adjusted to a constant particle number (CN). To test whether single particle detection is possible, a titration series of 60- to 80-nm-sized nanoparticles was performed, of which single particle visibility was implicated by the previous experiment. Subsequently, these AuNPs were coincubated with a cultured cell line to study the intracellular visualization and quantification of laser-generated AuNPs. Quantitative mass spectrometry for the determination of gold allowed for an independent verification of the microscopic data.

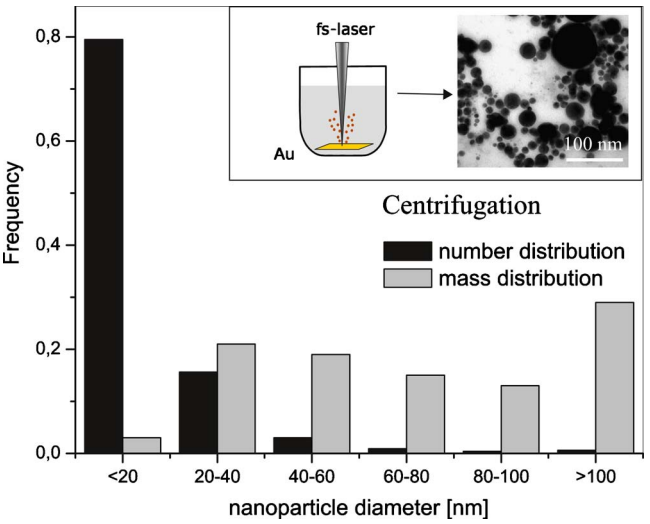

Fig. 1 Number- and mass-weighted size distribution of laser-generated gold nanoparticles in water estimated by centrifugation. Insert: scheme of nanoparticle generation by laser ablation in liquids and representative transmission electron micrograph of nanoparticles prior to centrifugation.

2 Methodology

2.1 *Generation and Examination of Gold Nanoparticles*

The applied laser-based approach to nanoparticles consists in the ablation of a target in liquid media by intense laser radiation, leading to an ejection of its constituent and the formation of a colloidal nanoparticle solution.[14,15] In the study at hand, AuNPs were generated using a femtosecond laser system (Spitfire Pro, Spectra-Physics, Santa Clara, California) delivering 120-fs laser pulses at a wavelength of 800 nm (maximum energy 400 μJ per pulse, beam diameter 4 mm). The pulse energy was fixed to 200 μJ at a repetition rate of 5 kHz. The principle setup is described as follows. The laser beam was focused on 5×5-mm gold foil (99.99% purity), thoroughly cleaned and placed on the bottom of a Petri dish filled with 4-mL bidistilled water. The plate was placed on an axis system that moved at a constant speed of 1 mm s^{-1} in a spiral with outer radius of 2 mm and inner radius of 0.4 mm. Time of irradiation was fixed to 12 min corresponding to three spirals.

The resulting colloid was characterized by UV-visual spectroscopy using a Shimadzu 1650 (Shimadzu Europe GmbH, Duisburg, Germany) and TEM (EM 10 C electron microscope, Zeiss, Oberkochen, Germany).[4,16] 500 nanoparticles were counted for the determination of the average Feret diameter (Fig. 1). AuNP concentration was estimated by weighing (Sartorius M3P-000V001, Sartorius AG, Göttingen, Germany) the gold foil three times prior and after laser ablation with an accuracy of 1 μg.

2.2 *Nanoparticle Size Separation*

Size separation of AuNPs was performed via successive centrifugation steps of 500 μL of the colloid with a Hellma Universal 320 centrifuge Rotor 1612. The time of centrifugation (t) was fixed to 15 min, and the rotation velocity (v) was calculated via Eq. (1) (for detailed values see Table 1).

$$v = \frac{60}{2\pi}\sqrt{\frac{\ln\left(\frac{x}{x_m}\right)}{ts}}, \tag{1}$$

where x is the radius bottom, x_m is the radius meniscus, and s is the sedimentation coefficient.

The supernatant was separated from the pellet and used for the following centrifugation step. The pellet was redispersed in 100-μL H_2O, and size distributions and optical properties were characterized by dynamic light scattering and UV-visual spectroscopy, respectively.

Nanoparticle mass concentrations (c_m) were estimated via recorded intensities at 380 nm, which were converted by interpolation from a linear standard calibration curve. The wavelength of 380 nm corresponds to the interband transition of gold and is hardly affected by nanoparticle size, shape, and environment. The number concentration (c_n) was subsequently calculated via Eq. (2) assuming a density of GNPs of $p=19.3$ g/cm^3, where r is the mean radius of each group.

Table 1 Centrifugation parameters for nanoparticle size separation ($t=15$ min each).

Size class [nm]	rpm [min^{-1}]
>100	1500
80 to 100	1800
40 to 60	2500
20 to 40	7000
<20	supernatant 7000

Table 2 Size-dependent reciprocal relationships of AuNP mass and particle number.

Diameter (nm)	Particle mass (P_m) in fg	Number of AuNPs in 500 fg
15	0.03414	14645.57
20	0.08093	6178.38
40	0.64742	772.30
50	1.26449	395.42
60	2.18504	228.83
70	3.46976	144.10
80	5.17935	96.54
100	10.11592	49.43
200	80.92736	6.18

$$c_n = \frac{3c_m}{4\pi r^3 \rho}. \quad (2)$$

Two different size-separated series were established. While one of them was adjusted to constant particle mass concentrations (50 μg/mL respective 250 μM Au=CM), a second series was adjusted to constant particle number concentrations ($1*10^{10}$ AuNP/mL=CN).

2.3 *Preparation of Gold Nanoparticles in Dispersion for Laser Scanning Confocal Microscopy Analysis*

Colloidal AuNPs of each of the size fractions of both series were analyzed in 0.5-μL ddH_2O resting in a 5-μL silicon oil cushion. All colloids were sealed under a cover slip. Imaging was performed within two hours after preparation.

Thus the number of particles included in each size fraction within CM increased with decreasing particle size (Table 2). In CN, particle fractions consist of decreasing masses with smaller sizes (Table 2).

2.4 *Cell Culture and Preparation for Laser Scanning Confocal Microscopy Analysis*

The cells used in the coincubation studies were derived from a bovine immortalized endothelial cell line (GM7373) obtained from the Cell Culture Collection, Institute of Infectology, FLI, Riems, Germany). Cell growth conditions and postcoincubation treatment corresponded to previously described trials.[4] For LSCM analyses, these prepared cells were mixed 1:4 with Vectashield (Axxora, Loerach, Germany) and mounted on a slide within a paper reinforcement ring sealed by a cover slip and nail varnish.

2.5 *Gold Nanoparticle Coincubation Assays*

Coincubation assays were performed using AuNPs in a final concentration of 50 μM. After seeding, cells were allowed to attach and were then exposed to the nanoparticles for 48 h. The added AuNPs displayed either the complete size range with an average particle diameter of 15 nm or separated size fractions of 40 to 60 nm and 60 to 80 nm, respectively. Cells incubated without AuNPs for 48 h were used as controls. All experiments were carried out in duplicates and repeated three times.

2.6 *Imaging by Laser Scanning Confocal Microscopy*

Visualization was carried out with a confocal laser scanning system LSM510 at an Axioplan 200 (Carl Zeiss MicroImaging GmbH, Jena, Germany) within the spectrum of visible light. Laser wavelengths of 514 nm (argon, 15 mW), 543 nm (helium neon green, 1 mW), and 633 nm (helium neon red, 5 mW) were used to excite the SPR or luminescence of the colloidal AuNPs and the AuNPs in cultured bovine cells. Light scattering for each of the excitation wavelengths was recorded in multitracking mode in combination of four separate detection channels within fixed spectral bands. Complete configurations are summarized in Table 3. The colloidal AuNPs were investigated dispersed in bidistilled water using the configurations described in Table 3. After focusing the edges of the silicone oil cushion, a volume of 10 pL centered within the liquid volume, avoiding reflections at the surfaces by exclusion of 2 to 3 μm next to each glass, was imaged. The focus of cells was adjusted using the differential interference contrast (DIC) contrast as reference.

2.7 *Statistics*

Statistical analyses were performed with the software SigmaStat 3.0 (StatCon, Witzenhausen, Germany). Quantification of LSCM data was performed on five repetitive measurements for the colloidal nanoparticles and ten fields of view for each of the size groups of the AuNPs in cells. Data of reflecting pixel numbers were normalized by square root transformation and were applied to one-way analysis of variance with the pair-wise multiple test by Holm-Sidak ($p=0.05$).

2.8 *Mass Spectroscopic Quantification of Gold in Bovine Immortalized Cells*

The summarized analysis of the gold concentration in the cells was performed by inductively coupled plasma mass spectrometry (ICPMS) by a certified laboratory (Wessling GmbH, Hannover, Germany). Samples of 200 μL containing approximately 3×10^6 cells were analyzed. The particle numbers (Np) were calculated using the sample-specific cell numbers (n_c) and the mass of gold within the sample (m_{au}) for each group using Eq. (3). P_m refers to the mean particle masses within the groups.

$$Np = \frac{m_{au}10^6}{n_c P_m}. \quad (3)$$

3 Results and Discussion

3.1 *Physicochemical Characterization of Gold Nanoparticles*

The laser-generated aqueous gold colloid is characterized by a broad size distribution, covering the range of 3 to 200 nm with an average diameter of 15 nm as determined by transmission electron microscopy (Fig. 1, insert). The size classi-

Table 3 Configurations for surface plasmon resonance (SPR) and luminescence detection of AuNPs. Laser power is measured at the object level with 100% laser output. Laser power at 0.54 has performance at 5.9A.

Excitation wavelength (nm)	Detection	Laser power (mW)	Main beam splitter	Detection bandpass (nm)	Detection channel	Detection gain	Detection offset
514	Scattered SPR	0.54	80/20	505 to 545	3	250 to 400	−0.02
543	Scattered SPR	0.11	80/20	530 to 550	2	250 to 400	−0.02
633	Scattered SPR	0.53	80/20	>585	1	250 to 500	−0.05
514	Luminescence	0.54	488/543/633	530 to 570	2	700 to 800	−0.03
543	Luminescence	0.11	488/543/633	545 to 570	3	700 to 800	−0.05
633	Luminescence	0.53	488/543/633	>635	1	700 to 800	−0.1
633	Differential interference contrast (DIC)	0.53	488/543/633	None	Transmission	250 to 300	−0.5

fication by centrifugation reveals that the mass-weighted distribution is centered at around 50 nm, while the resulting number-weighted distribution shifts to smaller nanoparticles (Fig. 1). More than 80% of the nanoparticles seem to have a size of less than 20 nm.

In accordance with the Mie theory,[17] UV-visual spectra of the size fractions reveal a red shift and a broadening of the SPR with increasing mean diameter (Fig. 2). By normalizing the size fractions to a constant nanoparticle number of 10^{10} AuNP/mL, one additionally observes a significant intensity enhancement of the SPR for bigger nanoparticles. The

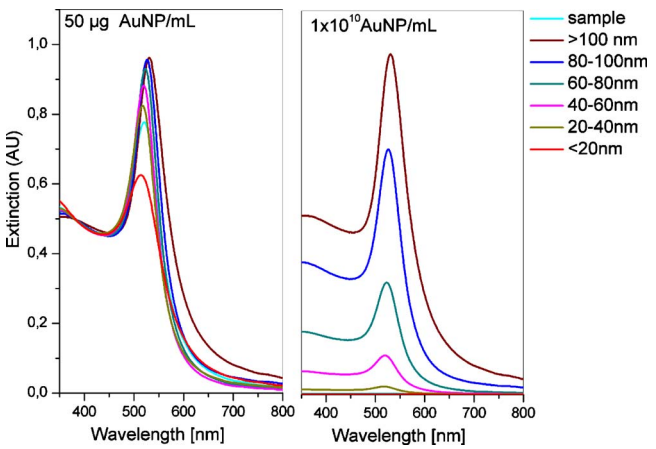

Fig. 2 UV-visual spectra of gold nanoparticle size fractions after centrifugation normalized to constant nanoparticle mass concentrations of 50 μg/mL (CM, left) and constant nanoparticle number concentrations (CN=10^{10} AuNP/mL, right).

SPR of nanoparticles with a diameter of less than 20 nm is thus hardly visible. This fact can be explained by the higher extinction coefficient of bigger nanoparticles and is even detectable when adjusting the fractions to a constant nanoparticle mass, although the nanoparticle number is significantly lowered with increasing diameters (Table 2).

3.2 *Visualization of Size-Restricted Colloidal Gold Particles by Laser Scanning Confocal Microscopy*

Representative images taken of a volume of about 10 pL ($31.3 \times 31.3 \times 10.21$ μm) of colloidal AuNPs of each size group of CN and CM are shown in Figs. 3(a)–3(d) and Figs. 3(f)–3(i), respectively. The number of particles contained in the visualized volume of about 10 pL of each fraction of CM was calculated using the average diameter and is added in Figs. 3(a)–3(d). As the particles were not fixed on the glass surface, the appearing irregular arrays of pixels could reflect the Brownian motion of diffusing particles. Time series after single laser excitation, reduced field of view (2.4 pL), and short exposure times 3 μs/pixel) verified this assumption.[18] As these arrays reflect single particles, counting of the pixels provides a good indication of particles accessible to objective image analysis although the pixel numbers are higher than the number of particles contained in the sample.

Interestingly, and probably due to differences in size or arrangement, a part of single objects in the samples seem to reflect selectively one or the other excitation wavelength, while others show colocalization of reflection of the different excitation wavelengths. Thus, the quantification of the numbers of reflecting pixels was performed for each of the three

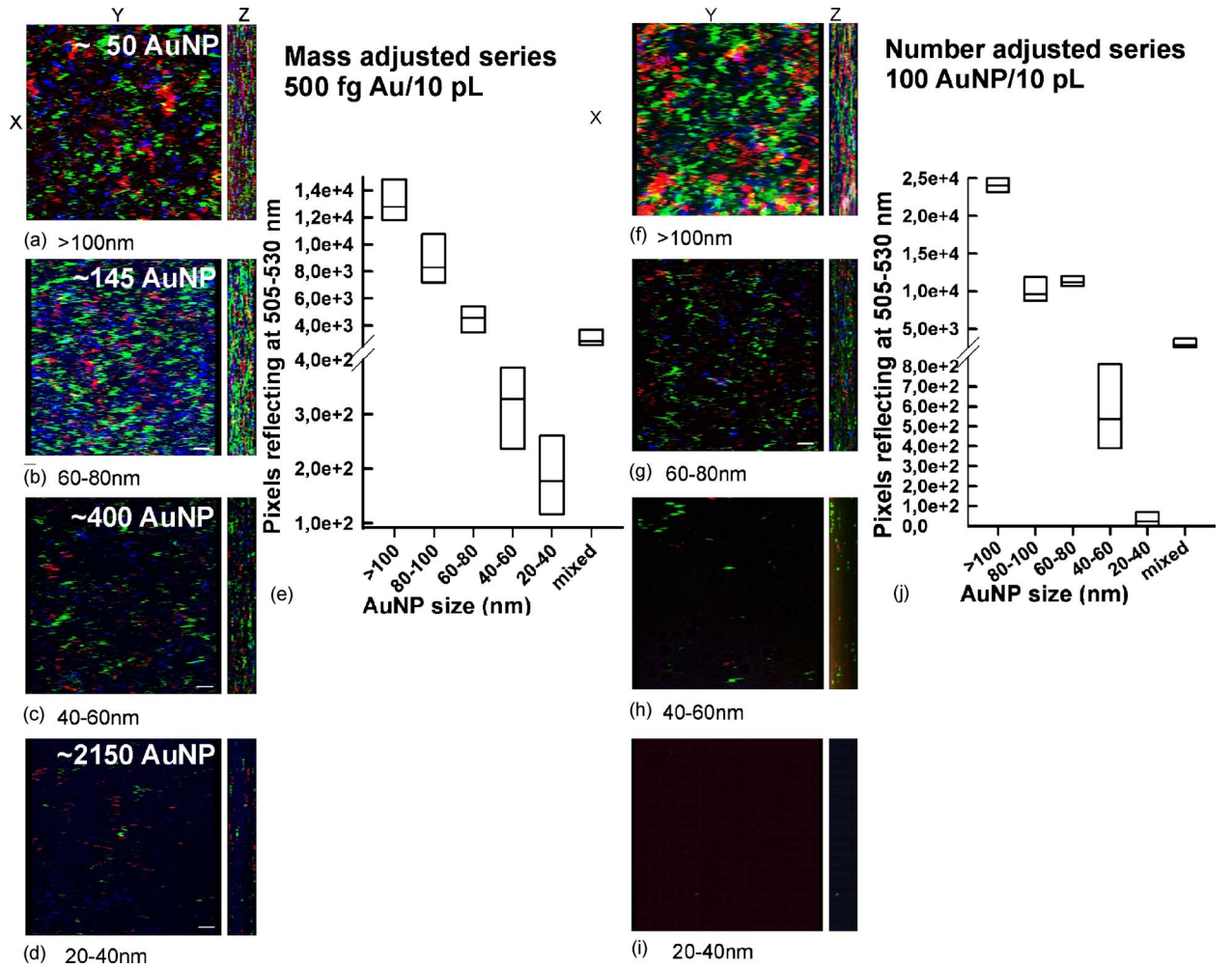

Fig. 3 Representative images of size-restricted AuNPs in 10-pL volumes ($31.3 \times 31.3 \times 10.21$ μm). (a) through (e) show images from mass-constant dispersions (CM). (f) through (j) show all colloids which were set to an equal number of AuNPs independent of their size (CN). Size of AuNPs was >100 nm in (a) and (f); 60 to 80 nm in (b) and (g); 40 to 60 nm in (c) and (h), and 20 to 40 nm in (d) and (i). Excitation was performed at 514, 543, and 633 nm with the corresponding SPR shown in blue, green, and red, respectively. Pixel size is $80 \times 80 \times 700$ nm, and pixel time is 5.44 μs. The box plots in (e) and (j) represent the median with 25 and 75% quartils of reflecting pixels in each of the size classes after excitation at 514 nm, scale 1 μm. (Color online only.)

detection bandpasses and in both series of size-separated colloidal AuNPs.[18] The SPR was shown previously quantified for all three reflection channels of CM (see Fig. 3 of Ref. 18). Exemplarily, the data from the excitation at 514 nm are shown [Figs. 3(e) and 3(j)] as they accounted for the highest number of pixels due to the proximity to the reflection maximum of gold.

Dispersions with constant particle mass (500 fg Au/10 pL) contain an increasing number of particles with decreasing diameter. Microscopic visualization reveals this number increase for the 100- to 80-nm (data not shown) and 80- to 60-nm samples compared to AuNPs >100 nm. However, patches of AuNPs >100 nm [Fig. 3(a)] appear bigger than the 80- to 60-nm sized particles [Fig 3(b)], resulting in a higher pixel count for the >100-nm fraction [Fig. 3(e)]. This probably reflects the size difference, as the reflection of particles in the >100-nm fraction might occupy more than one pixel. Particles 40 to 60 nm in diameter only provide a reduced number of reflective spots [Fig. 3(c)], and from the particles 20 to 40 nm only single objects contained signal intensities sufficiently high for microscopic detection, despite the 2150 particles included in the visualized volume [Table 2 and Fig. 3(d)]. From AuNPs smaller than 20 nm, no reflection could be recorded (data not shown). Thus, the reduced extinction of particles smaller than 60 nm measured by UV-vis spectroscopy (Fig. 2) can be correlated with a loss in scattering cross section, confirmed via limited microscopic imaging of these particles. Interestingly, all these findings result in a rather continuous decrease of pixel counts with decreasing particle diameter within CM. In contrast, a sharp drop of reflection was recorded between 60- to 80- and 40- to 60-nm sized particles in all three evaluated spectral bands in CN, confirming the incomplete detection of single particles with a diameter <60 nm. In the CM, this reduction of the scattering cross sections with reduced particle size is counteracted by the higher particle numbers and higher proximity of the single particles that enhanced the total reflection. However, it must be recognized that in this case, a bulk of particles adds up to

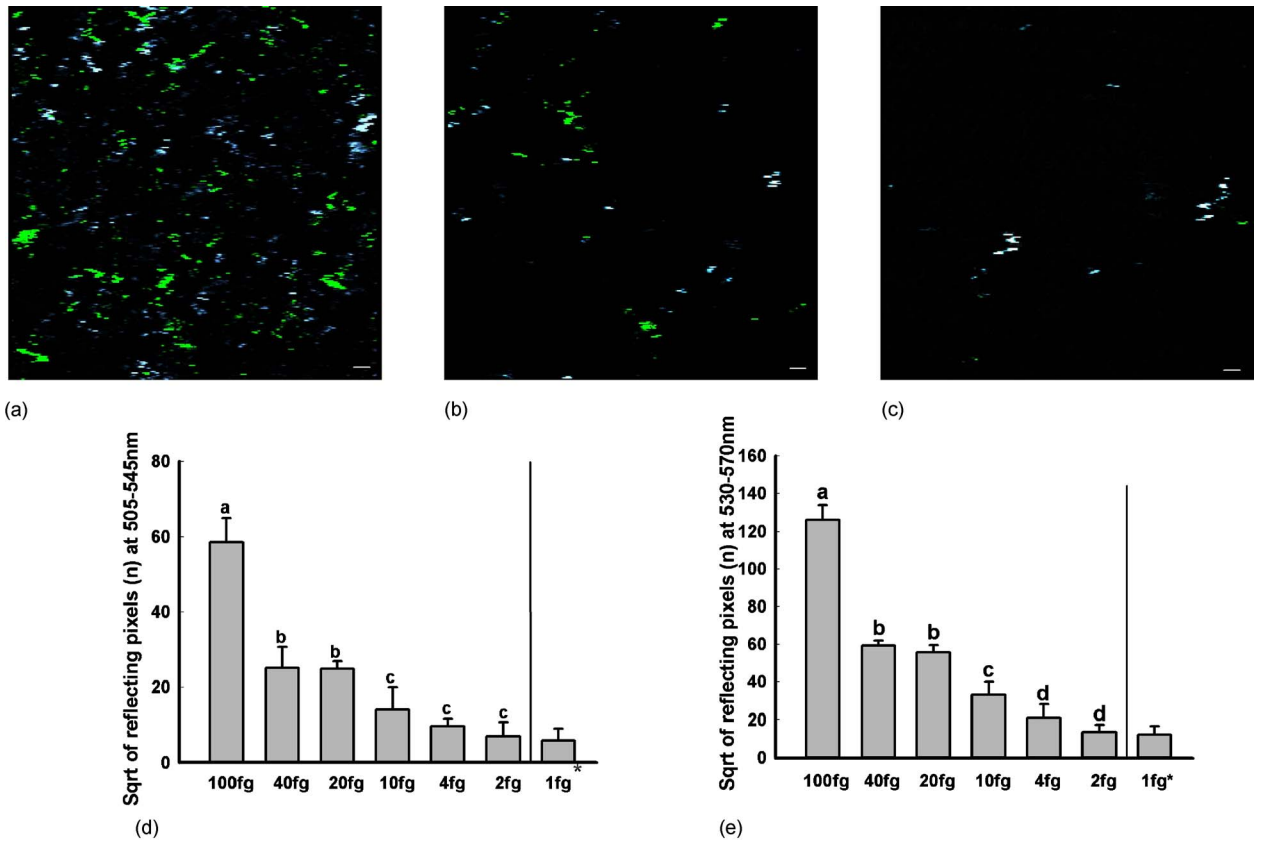

Fig. 4 (a), (b), and (c) are representative images and (d) and (e) are statistical ANOVA results of square root transformed reflecting pixel numbers in dilution series of AuNPs (60 to 80 nm). (a) represents a particle concentration of 100 fg/10 pL, (b) stands for 10 fg/10 pL, and (c) for 2 fg/10 pL. The square root transformed pixel numbers (d) and (e) correspond to the expected reduction of pixels from separate detection of single nanoparticles only in the more diluted samples. Pixel size is $80 \times 80 \times 700$ nm, pixel time is 4.32 μs, image is $25 \times 25 \times 10$ μm, and scale 1 μm. Asterisks show colloids of the 1-fg dilution that provided reflection only after increased detection gains and were excluded from the statistics.

one reflective spot. Furthermore, in the smaller particle groups [Figs. 3(c) and 3(d)], reflection was dominant at 543-nm excitation (green), indicating preferential detection of aggregated particles having a phase shift of their SPR to longer wavelengths.[1,2,6,12,19,20] In both series, only the group of 60- to 80-nm sized AuNPs [Fig. 3(b) and 3(g)] shows intensive reflection in all three bandpasses. In groups of particles >100 nm [Figs. 3(a) and 3(f)], the red band provides the largest clusters, although the total number of pixels reflecting in this bandpass comprises only about 10 to 20% compared to 514- and 543-nm excitation.

To conclude, visualization of colloidal AuNPs seems to be possible down to particle sizes of 60 nm, while for fixed nanoparticles the visualization of single 40- to 60-nm sized AuNPs has been reported. Additionally, a broadened absorption spectrum was seen for these surface-spotted AuNPs as described by others.[2,3] Doublets of single spherical AuNPs are frequently detectable in TEM images[9,21] and could be suggested from the shape of reflective spots we observed from surface-spotted particles in our study.[18] This arrangement could also explain the improved imaging of fixed particles in other studies.[9,12] Furthermore, spectral luminescence of AuNPs (size 50 nm $\pm$ 15%), spotted on a glass slide, was previously reported by Geddes et al.[9] However, from our data, luminescence could not be visualized from colloids of the 60- to 80-nm sized group.

The missing reflection of particles sized smaller than 20 nm and severe reduction of visibility of particles between 20 and 40 nm is in agreement to the very low scattering previously described.[1,12] Measuring the SPR-enhanced absorption would therefore be necessary to visualize these size ranges below 40 nm for quantification.[12]

3.3 *Quantification of Titrated* 60- to 80-nm *Colloidal Gold Nanoparticles by Laser Scanning Confocal Microscopy*

To verify whether single particles or clusters of particles were imaged, a volume of 10 pL ($31.4 \times 31.4 \times 10.2$ μm) of a dilution series from the AuNPs (60 to 80 nm) was excited with laser wavelengths at 514, 543, and 633 nm, and the reflecting pixels were counted. The stock dispersion of 100 fg/10 pL was diluted down to 1 fg/10 pL in six steps. In the 1-fg/10 pL dilution, only one out of ten fields of view provided a signal from four AuNPs. The detection gain was increased by 15% to allow for detection of very low reflecting spots. Therefore, this dilution step was not included in the statistical analysis; however, the data for this group are shown

in Figs. 4(d) and 4(e). However, as the particle mass of single particles sized 70 nm is 3.47 fg, the detection of four reflecting spots in one out of ten fields of view fits nicely with the expected appearance of one particle in about 40 pL of this dilution, and proved the detection of single particles of 60- to 80-nm size by confocal microscopy.

The minimum pixel size from 80×80 nm up to 220×220 nm applied in the current study is not suited to reflect the true size differences of AuNPs between 40 to 100 nm. Moreover, a summary of pixels at one position might reflect agglomerates of AuNPs[1,2] or the pathway of a single particle moving freely in aqueous environment during acquisition (Fig. 3). Thus, single particle detection is most accurate for AuNPs of 60 to 80 nm, if the interparticle distance is high enough to separate the signals of two individual AuNPs (Fig. 4).

3.4 *Visibility of Gold Nanoparticles after* 48-hours *of Coincubation within Bovine Immortalized Cells and Mass Spectrometric Validation*

The potential of conventional confocal microscopy to quantify AuNPs was reinvestigated in bovine immortalized cells that had been coincubated with AuNPs for 48 h. Reflection intensity increased in the cellular environment, and the spectral characteristics were shifted to longer wavelengths. Luminescence was not recorded after excitation at 543 or 633 nm from colloidal AuNPs, but was apparent from AuNPs within cells (Fig. 5). Although due to the cellular background, the detection offset was raised for the discrimination of AuNPs within cells and the gain reduced, the recorded intensities of reflection increased for all bands of detection.

Imaging conditions were optimized for dispersed AuNPs achieving 100 to 200 gray values as background and avoiding intensities above the differentiation range. Typical intensity distributions are demonstrated in supplementary information (Figs. 6 and 7). Only pixels with intensities above 700 were included in the quantification to ensure a signal-to-noise ratio (SNR) above 3. Signals with low intensities were recorded typically above 1000, but most spots reached intensities of 2000 to 3500 from 4096 gray values.

The localization of AuNPs in cells appears to inhibit the free movement of AuNPs as seen in colloids, and thus enables counting of reflecting objects instead of pixels in cells [Figs. 5(d)–5(f)]. This confirms previous data where the enclosure of single AuNPs in distinct electron dense structures after diffusion in the cells was demonstrated.[4] Moreover, a high degree of colocalization for the different reflection bands was obvious in contrast to the dispersed particles. Although reflection bands of 505 to 545 and >585 nm were recorded for the dispersed AuNPs as well as from the cells, AuNPs were provided only from cell reflection signals and additional detectable luminescence signals from the longer wavelengths, indicating a further red shift of the SPR due to the increased refractive index of the cellular environment.

The impressive SNR and stability of the reflection compared to the fading of fluorescence dyes is further augmented if the unfixed cells, washed only once in phosphate buffered saline (PBS), were investigated (Fig. 8). Low excitation of autofluorescence within the reflection bandpass enabled similar clear differentiation of the AuNPs within the cells.

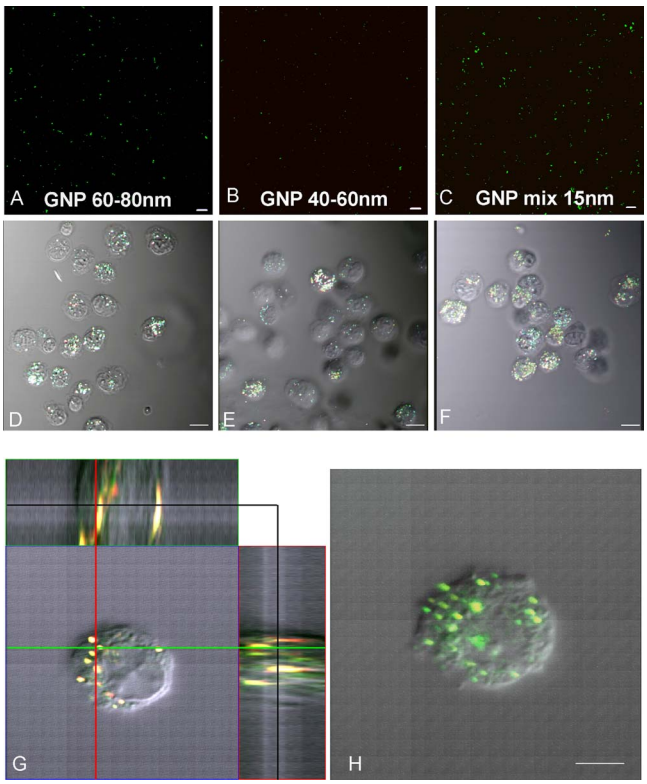

Fig. 5 Size restricted AuNPs (10-mM Au) of a mixed sample with mean particle size of 60 to 80 nm [(a) and (d)], size selected AuNPs of 40 to 60 nm [(b) and (e)], and of 15 nm [(c) and (f)] are visualized as colloids in ddH_2O [(a) and (c)] and after 48 h of coincubation in GM7373 cells [(d), (e), and (f)]. Pixel size is $90 \times 90 \times 600$ nm, pixel time is 1.28 μs, and image is $33 \times 33 \times 12$ μm. The figures show the overlay of four imaged channels each. The dispersed AuNPs were visualized in reflection bands after excitation at 543 and 633 nm, respectively, and two luminescence bands (at 543-, and 633-nm excitation) as described in Table 3. However, exclusively SPR was visualized from the dispersed AuNPs of all size groups resulting in the green dominated false color images. The AuNPs in cells [(d), (e), and (f)] are shown as an overlay of reflection after 543-nm excitation, and luminescence after 543-nm and 633-m excitation added to the DIC transmission defining the position of the single cells. The orthogonal views at a single optical slice of the series of 900-nm-thick optical sections through a single cell (g) in comparison to the 3-D projection of this cell (h) indicate the within-cell location of several nanoparticles, scale 5 μm. (Color online only.)

After the 48-h coincubation period with AuNPs sized 60 to 80 nm, a median of 11.6 particles per cell was found in 100 cells (Table 4). Coincubation of cells with the mixed size sample (average particle diameter 15 nm) and AuNPs sized 40 to 60 nm resulted in particle numbers with a median of 13.8 and 9.1 particles per cell, respectively. As an independent verification of the microscopically counted number of AuNPs inside cells, gold mass spectrometry was performed from a fraction of the same cell cultures. The number of particles recalculated from the total mass of gold found in approximately 3×10^6 cells confirmed that the particle counts for the size group of 60 to 80 nm, retrieved from the microscopic evaluation, were accurate (Table 4). These data also revealed by this visualization independent measure that particles smaller than 60 nm were only incompletely visualized by

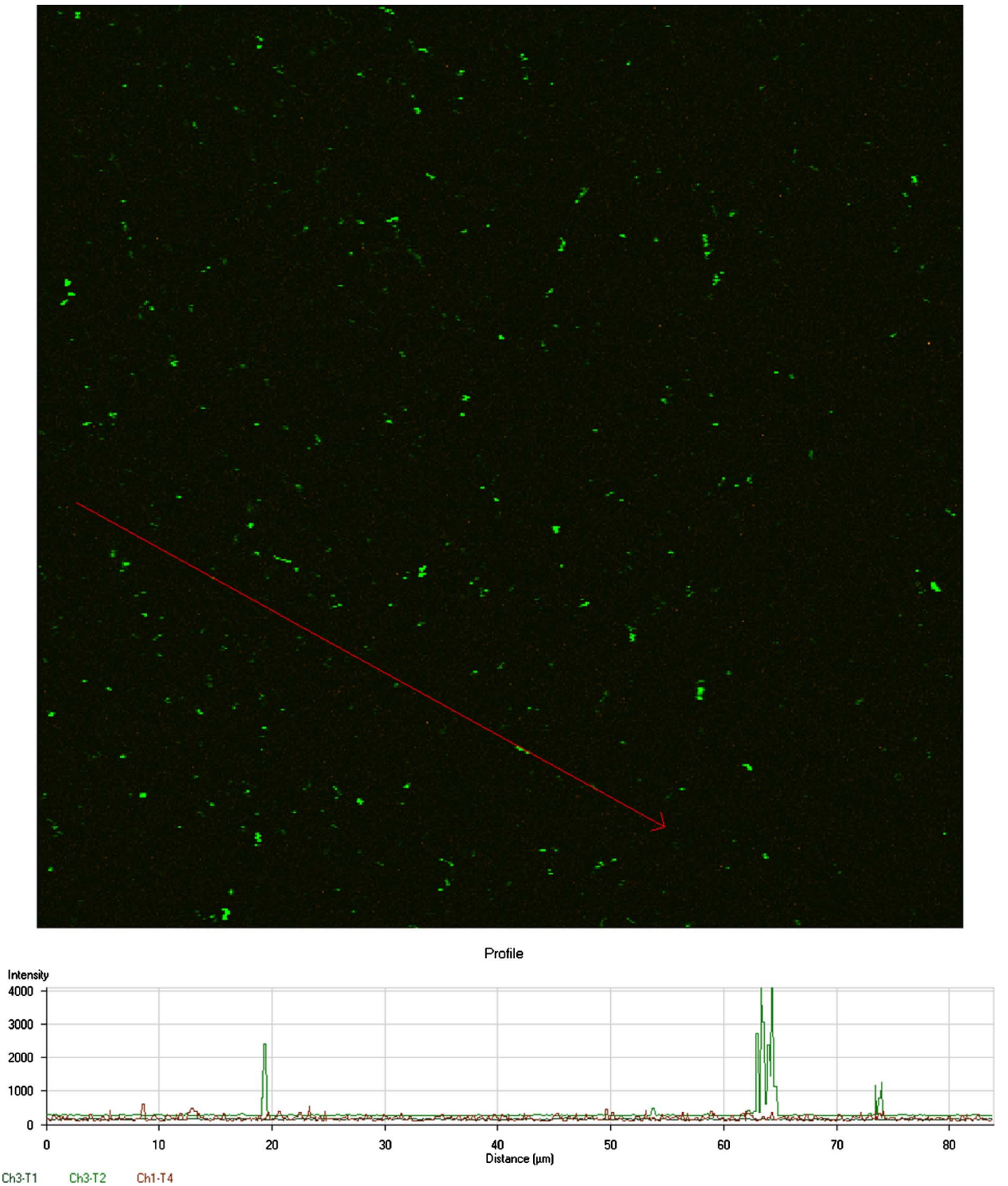

Fig. 6 Intensity profiles of three channels from the volume of 10 pL, including dispersed 60- to 80-nm AuNPs of Fig. 5(a). The green line represents SPR after excitation at 514 nm. The background values of the blue and red lines were recorded in the luminescence mode after 514- and 633-nm excitation. (Color online only.)

confocal microscopy. A mean of nine particles could be counted, but a mean 27 particles per cell had been calculated from the mass spectrometry in the sample incubated with particles of 40 to 60 nm diameter. Especially for the size group of about 15 nm, only a minute number of the AuNPs that penetrated the cells were detected microscopically by their scattering cross sections. Only 13.8 spots per cell were visualized; however, 8634 particles per cell must have been present within the cells according to the mass spectrometric data recorded from the same cell culture (Table 4).

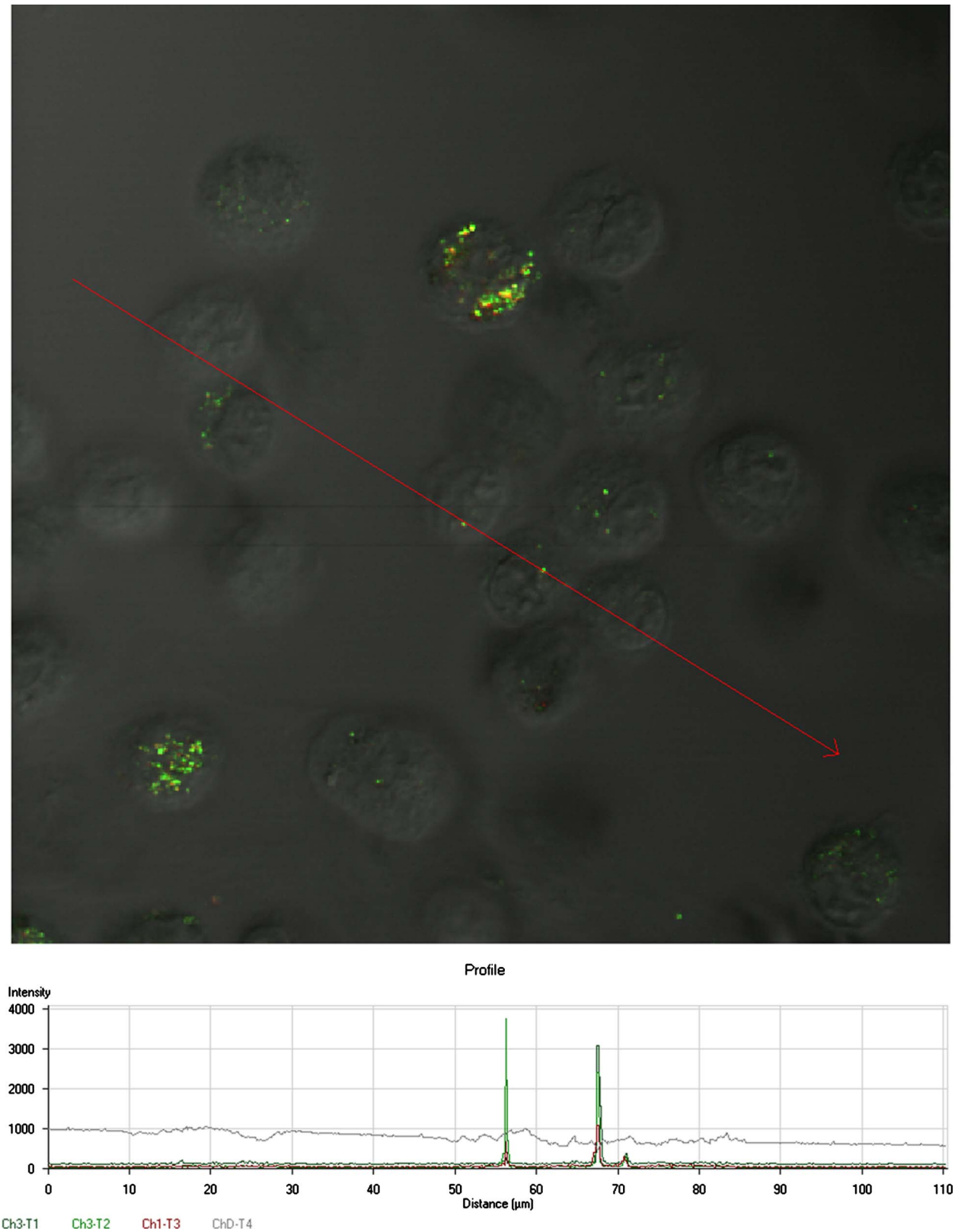

Fig. 7 Intensity profiles of four channels from a single optical slice of a Z-series through cells demonstrated as 3-D projection in Fig. 5(d). The green line represents SPR after 514-nm excitation. Within the cells, additional signals were recorded from the same AuNPs in luminescence after excitation at 514 and 633 nm. The gray line corresponds to the DIC transmission. (Color online only.)

Table 4 Mass spectrometric and microscopic quantification of gold (Au) in cells coincubated with AuNPs of different size classes. The asterisk indicates cells had been counted in individual samples after coincubation in uniform 3 mio cells/ml and final processing.

AuNP size (nm)	Mass spectrometry				Microscopic cell counts particles/cell (median of 100 cells; 25 and 75% quartiles)
	Cells ($n/\mu L$)*	Mass Au (ng/μL)	Mean particle mass (fg)	Particles/cell calculated	
15	9061	2.671	0.03414	8634	13.8 (9,4; 15.9)
40 to 60	17005	0.583	1.26449	27	9.1 (4.5; 11.9)
60 to 80	16750	0.598	3.46976	10	11.6 (9.4; 15.9)

Taking into account that the colloid AuNPs could not be detected if they had been smaller than 40 nm, it is somewhat surprising that we saw any particles in the mixed AuNP group with a mean of 15 nm diameter. One possible explanation is that the detected particles could be the few AuNPs of bigger size, which are to be expected in this group. On the other hand, signals detected with the microscope could also have come from agglomerated nanoparticles.

It was also surprising that ICPMS analysis found such tremendous amounts of particles with mean diameters of 15 nm inside cells. Previous studies[22] have indicated the best penetration efficiency for 50-nm AuNPs compared to smaller ones. However, in those cases, no visualization independent measure of AuNPs was evaluated. Nevertheless, our previous studies revealed diffusion as the most probable mechanism for cellular uptake of unconjugated, laser-generated AuNPs.[4] The different surface characteristics of laser-generated AuNP in contrast to chemically synthesized ones might also be responsible for these differences in cell penetration.

Diffusion, a main pathway for cell penetration, was not discussed yet for AuNPs. Instead, endosomal pathways were presumed as uptake mechanisms of these gold nanoparticles into the cells. Taylor et al.[4] demonstrated diffusion as the most feasible mechanism for cell penetration of the unconjugated AuNPs. As all the size-restricted samples of unconjugated laser-generated AuNPs appear in small discrete signals throughout the cells, the presence of oxidized Au^{+} and Au^{3+} providing a positive surface charge might be responsible for this unique behaviour.

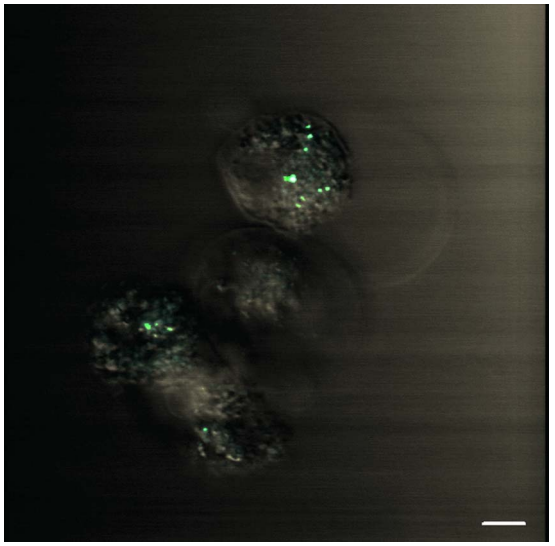

Fig. 8 Cells coincubated with 60- to 80-nm sized AuNPs for 48 h. Visualization was performed from unfixed cells washed once in PBS and mounted in Vectashield. Scale 5 μm.

4 Conclusions

The investigation of size-separated colloids of laser-generated gold nanoparticles clearly show unrestricted visibility of AuNPs of 60 nm and larger by confocal laser scanning microscopy. The scattering cross section of SPR for particles of this size can be visualized to the single particle level. A cumulative effect of scattered light from several single particles or formation of aggregates is necessary to provide detectable scattering cross sections in the groups with 40 to 60 nm and 20- to 40-nm AuNPs. Larger AuNPs are difficult to separate as colloids. Interestingly, colloidal AuNPs reflect different spectral bands within the same size group. Inside cells, the AuNPs sized 60 to 80 nm can also be quantified in distinct compartments with a high chance of single particle separation. Within cells, a spectral shift to longer wavelengths is seen and the AuNPs gain additional luminescence that could be used for visualisation (Fig. 5).

The defined size-dependent optical detection limit of spherical AuNPs could thus be used for status-dependent visualization of AuNPs. As conjugated laser-generated AuNPs are clearly reduced in their size range to about 5 nm in total,[5] these functionalized AuNPs are not accessible to light microscopic detection by their scattering cross sections. However, after clustering of a few single particles, for instance at a hybridization focus, the successful hybridization could be recorded without any washing of nonhybridized particles. This would provide one further important characteristics for applications in living biosystems.

Acknowledgments

The project was supported by the excellence cluster REBIRTH, Masterrind GmbH Verden, and the NBank Niedersachsen.

References

1. S. Link and M. A. El-Sayed, "Size- and temperature dependence of the plasmon absorption of colloidal gold nanoparticles," *J. Phys.*

Chem. B **103**, 4212–4217 (1999).
2. S. Link and M. A. El-Sayed, "Optical properties and ultrafast dynamics of metallic nanocrystals," *Annu. Rev. Phys. Chem.* **54**, 331–366 (2003).
3. P. K. Jain, I. H. El-Sayed, and M. A. El-Sayed, "Au nanoparticles target cancer," *Nanotoday* **2**, 18–29 (2007).
4. U. Taylor, S. Klein, S. Petersen, W. Kues, S. Barcikowski, and D. Rath, "Non-endosomal cellular uptake of ligand-free, positively charged gold nanoparticles," *Cytometry* **77a**, 439–446 (2010).
5. S. Petersen and S. Barcikowski, "*In situ* bioconjugation: single step approach to tailored nanoparticle-bioconjugates by ultrashort pulsed laser ablation," *Adv. Funct. Mater.* **19**, 1167–1172 (2009).
6. M. A. Van Dijk, A. L. Tchebotareva, M. Orrit, M. Lippitz, S. Berciaud, D. Lasne, L. Cognet, and B. Lounis, "Absorption and scattering microscopy of single metal nanoparticles, *Phys. Chem. Chem. Phys.* **8**, 3486–3495 (2006).
7. P. Zijlstra, J. W. M. Chon, and M. Gu, "Five-dimensional optical recording mediated by surface plasmons in gold nanorods," *Nature* **459**, 410–413 (2009).
8. M. Schmelzeisen, J. Austermann, and M. Kreiter, "Plasmon mediated confocal dark-field microscopy," *Opt. Express* **16**, 17826–17841 (2008).
9. C. D. Geddes, A. Parfenov, I. Gryczynski, and J. P. Lakowics, "Luminescent blinking of gold nanoparticles," *Chem. Phys. Lett.* **380**, 269–272 (2003).
10. G. Raschke, S. Kowarik, T. Franzl, C. Sönnichsen, T. Klar, and J. Feldmann, "Biomolecular recognition based on single gold nanoparticle light scattering," *Nano Lett.* **3**, 935–938 (2003).
11. M. Pelton, J. Aizpurua, and G. Bryant, "Metal-nanoparticle plasmonics," *Laser Photonics Rev.* **2**, 136–159 (2008).
12. K. Lindfors, T. Kalkbrenner, P. Stoller, and V. Sandoghdar, "Detection and spectroscopy of gold nanoparticles using supercontinuum white light confocal microscopy," *Phys. Rev. Lett.* **93**, 037401 (2004).
13. M. A. Van Dijk, M. Lippitz, and M. Orrit, "Far-field optical microscopy of single metal nanoparticles," *Acc. Chem. Res.* **38**, 594–601 (2005).
14. S. Barcikowski, A. Hahn, A. V. Kabashin, and B. N. Chichkov, "Properties of nanoparticles generated during femtosecond laser machining in air and water," *Appl. Phys. A: Mater. Sci. Process.* **87**, 47–55 (2007).
15. S. Petersen, J. Jakobi, A. Hortinger, and S. Barcikowski, "*In situ* conjugation—tailored nanoparticle-conjugates by laser ablation in liquids," *J. Laser Micro. Nanoeng.* **4**, 71–74 (2009).
16. S. Petersen, J. Jakobi, and S. Barcikowski, "*In situ* bioconjugation—novel laser based approach to pure nanoparticle-conjugates," *Appl. Surf. Sci.* **255**, 5435–5438 (2009).
17. G. Mie, "Beiträge zur optik über medien, speziell kolloidaler metallösungen," *Ann. Phys.* **330**, 377–445 (1908).
18. S. Klein, S. Petersen, U. Taylor, D. Rath, and S. Barcikowski, "Quantification of colloidal and intracellular gold nanomarkers down to the single particle level using confocal microscopy," in *Biomedical Applications of Light Scattering IV*, *Proc. SPIE* **7573**, 75730L (2010).
19. A. V. Kabashin and M. Meunier, "Synthesis of colloidal nanoparticles during femtosecond laser ablation of gold in water," *J. Appl. Phys.* **94**, 7941– (2003).
20. F. Mafune, J. Kohno, Y. Takeda, T. Kondow, and H. Sawabe, "Formation and size control of silver nanoparticles by laser ablation in aqueous solution," *J. Phys. Chem. B* **104**, 9111–9117 (2000).
21. C. D. Geddes, A. Parfenov, and J. R. Lakowicz "Luminescent blinking from noble-metal nanostructures: New probes for localization and imaging," *J. Fluoresc.* **13**, 297–299 (2003).
22. B. D. Chithrani, A. A. Ghazani, and W. C. W. Chan, "Determining the size and shape dependence of gold nanoparticle uptake into mammalian cells," *Nano Lett.* **6**, 662–668 (2006).